Supporting Information for: Ultrafast Nanoimaging of the Photoinduced Phase Transition Dynamics in VO_2

Sven A. Dönges,[1,*] Omar Khatib,[1,*] Brian T. O'Callahan,[1] Joanna M. Atkin,[2] Jae Hyung Park,[3] David Cobden,[3] and Markus B. Raschke[1]

[1]*Department of Physics, Department of Chemistry, and JILA, University of Colorado, Boulder, CO 80309*

[2]*Department of Chemistry, University of North Carolina, Chapel Hill, NC 27514*

[3]*Department of Physics, University of Washington, Seattle, WA 98195*

[*]These authors contributed equally to this work.

I. PUMP FLUENCE ESTIMATION

The pump fluences used in the experiment were calculated from the setup geometry for a Gaussian pump beam diameter of $r = 2.3$ mm and an angle of incidence on the sample of $\alpha = 26°$. With the focal length of the off-axis parabolic mirror $f = 11.25$ mm, and the wavelength of the pump light $\lambda_{\mathrm{NIR}} = 1032$ nm, the diffraction-limited pump spot size on the sample is calculated to be 6.2 μm. As the sample is not illumated at normal incidence the illumination spot becomes elliptical with the major half axis $a = 14$ μm. For an average pump power in the range of $P = 5$-13 mW incident on the tip, pulse energies between 5-14 nJ are achieved, yielding fluences of $F = 2$-5 mJ/cm^2 in the elliptical sample area illuminated by the pump beam. These are comparable to previously reported threshold fluences to induce the IMT in VO_2 [1], although on the lower end of the requisite fluence thresholds [2–5]. The pump fluence estimation here does not include any near-field enhancement of the tip, which we discuss below.

II. PUMP-PROBE SAMPLE VOLUME

An important consideration in ultrafast *s*-SNOM nanoimaging involves the effective pumped and probed sample volumes. In far-field pump-probe spectroscopy, a homogeneously excited probe region is desired, typically achieved by choosing a pump focus size exceeding the probe focus size to account for the pump beam profile. In *s*-SNOM, however, the pump excitation and probe volume can no longer be defined independently but are simultaneously determined by the apex size and associated spatial extent of the near-field. In this way, the entire pump-probe response is governed by the tip geometry, and both are localized to length scales set by the tip radius (10-20 nm).

Though the total probe response is a convolution over the spatial inhomogeneity of the pump excitation, the spatial near-field distribution of the probe itself makes the *s*-SNOM probe response more sensitive to the most localized and most strongly pumped near-field region in its center. Higher tip-harmonic demodulation ($n\omega_{tip}$), typically employed to reject far-field contributions to the signal, can further ensure a more highly localized probe volume. Figure S1a shows the distance dependence of the demodulated scattered signal at various harmonics n of the tip tapping frequency at temporal overlap $\Delta t = 0$ between the pump and

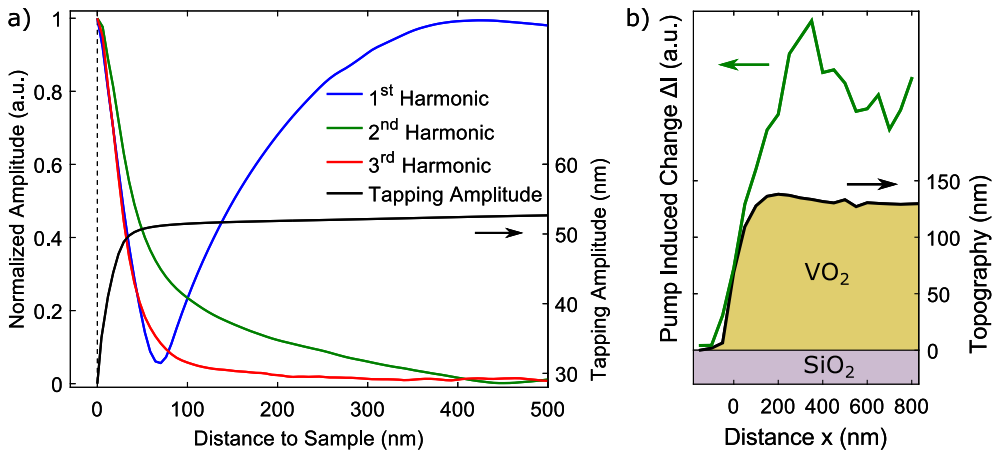

FIG. S1: Correlation of vertical and lateral near-field *s*-SNOM signal. (a) Near-field probe response approach curves after pump excitation, recorded on a VO_2 microcrystal at temporal overlap $\Delta t = 0$. (b) Time-integrated near-field probe profile of the line scan shown in Figure. 4a of the main text, indicating the total pump induced change in the near-field intensity as the AFM tip scans across the edge of the microcrystal.

probe. The scattered near-field intensity rises in close proximity to the sample, becoming more localized as n increases. The large variation seen for $n = 1$ is indicative of a far-field interference between incoming and outgoing fields, due to non near-field related scattering from the sample or tip shaft over the area of the laser focus. Typically $n = 2$ or 3 is sufficient to isolate the near-field response.

III. SELF-HOMODYNE PUMP-PROBE S-SNOM

In conventional *s*-SNOM extrinsic effects such as those described above are well understood, as well as complications due to different detection configurations [6–9]. The simplest modality is self-homodyne detection, as we employ here, where the back-scattered near-field is amplified by a local background reference field with an unspecified phase. Self-homodyne measurements have increased signal-to-noise and stability compared to other interferometric configurations that utilize an additional reference field. Though not explicitly near-field phase resolved, a self-homodyne *s*-SNOM measurement can in some instances even fully recover narrow vibrational and molecular resonances [10, 11], and is typically sufficient to register Drude amplitude contrast (with a slowly varying phase response), as established pre-

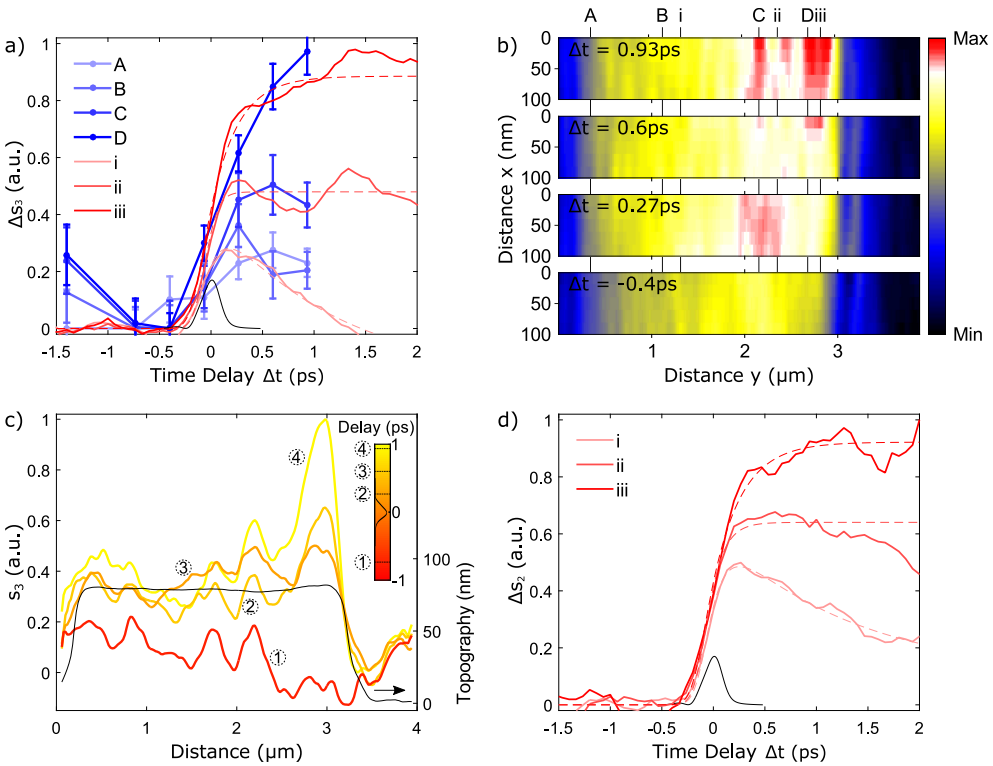

FIG. S2: (a) 3^{rd} Near-field pump-probe time traces recorded on different positions on a micro-crystal (red, positions indicated in b), together with full time traces extraced from a series of spatiotemporal images (blue, images and positions shown in b). (b) Set of images showing spatial and temporal variations in the IMT dynamics of a single VO_2 microcrystal. (c) Line profiles for several pump-probe time delays across the microcrystal shown in b. (d) Repeated time trace measurements obtained at positions (i)-(iii) indicated in b.

viously for VO_2 [12]. This is equally true for near-field pump-probe, especially for the case of our smooth single-crystalline VO_2 surfaces, as compared to more heterogeneous samples with a coexistence of many phases and local scatterers.

Signal demodulation at the 2$^{\text{nd}}$ harmonic ($2\omega_{tip}$) is often sufficient to isolate the near-field interaction, as seen in Figure S1a. Additionally, in Figure S2a-c we include the data recorded concurrently with the results presented in Figure 3 of the main manuscript, but with the signal demodulated at the 3$^{\text{rd}}$ harmonic of the tip frequency ($3\omega_{tip}$). Despite a much weaker signal and overall lower signal-to-noise, the data exhibit identical behavior and demonstrate the various IMT regimes detailed in the main text over the same few 100 nm spatial scale, indicating the nanoresolved photoinduced IMT dynamics. The time traces

shown in Figure S2d are repeated measurements at the positions indicated by (i)-(iii) in Figures 3b, S2b recorded at a later time in the experiment, to check both the temporal and spatial repeatability of our observations.

There are indeed new considerations that arise when including ultrafast pump pulses in the near-field interaction, as also emphasized recently in Ref. [13], where a time-dependent background field can introduce additional temporal or spatial variations. However such variations would likely manifest themselves in an artificial substrate 'pump-probe' response, especially close to the crystal edge, since an extended area is illuminated by the diffraction-limited pump beam. Figure S1b shows the time-integrated pump-probe response:

$$\Delta I = \int_{0\mathrm{ps}}^{2\mathrm{ps}} (\Delta s_2(\Delta t) - \overline{\Delta s_2}(\Delta t < 0))\, d\Delta t, \tag{1}$$

indicating the total pump induced change in the near-field intensity as the AFM tip moves across the edge of the microcrystal shown in Figure 4a of the main text. We see an abrupt rise in the total signal and a strong localization of the pump induced changes to the VO_2 microcrystal edge, and did not observe a pump-probe response on the substrate in any of our measurements. The high degree of localization shown in Figure S1b may also indicate that there is a moderate enhancement of the pump field of 2-5 by the tip, confining the photoinduced IMT near threshold only to the nanofocused volume beneath the tip apex.

---

[1] O'Callahan, B. T.; Jones, A. C.; Hyung Park, J.; Cobden, D. H.; Atkin, J. M.; Raschke, M. B. *Nat. Commun.* **2015**, *6*, 6849.

[2] Wall, S.; Foglia, L.; Wegkamp, D.; Appavoo, K.; Nag, J.; Haglund, R. F.; Sthler, J.; Wolf, M. *Phys. Rev. B* **2013**, *87*, 115126.

[3] Morrison, V. R.; Chatelain, R. P.; Tiwari, K. L.; Hendaoui, A.; Bruhcs, A.; Chaker, M.; Siwick, B. J. *Science* **2014**, *346*, 445–448.

[4] Cocker, T. L.; Titova, L. V.; Fourmaux, S.; Holloway, G.; Bandulet, H.-C.; Brassard, D.; Kieffer, J.-C.; El Khakani, M. A.; Hegmann, F. A. *Phys. Rev. B* **2012**, *85*, 155120.

[5] Cavalleri, A.; Dekorsy, T.; Chong, H. H. W.; Kieffer, J. C.; Schoenlein, R. W. *Phys. Rev. B* **2004**, *70*, 161102.

[6] Ocelic, N.; Huber, A.; Hillenbrand, R. *Applied Physics Letters* **2006**, *89*, 101124.

[7] Schnell, M.; Carney, P. S.; Hillenbrand, R. *Nat Commun* **2014**, *5*, 3499.

[8] Berweger, S.; Nguyen, D. M.; Muller, E. A.; Bechtel, H. A.; Perkins, T. T.; Raschke, M. B. *J. Am. Chem. Soc.* **2013**, *135*, 18292–18295.

[9] Muller, E. A.; Pollard, B.; Raschke, M. B. *J. Phys. Chem. Lett.* **2015**, *6*, 1275–1284.

[10] Craig, I. M.; Taubman, M. S.; Lea, A. S.; Phillips, M. C.; Josberger, E. E.; Raschke, M. B. *Opt. Express* **2013**, *21*, 30401–30414.

[11] Pollard, B.; Maia, F. C. B.; Raschke, M. B.; Freitas, R. O. *Nano Lett.* **2016**, *16*, 55–61.

[12] Jones, A. C.; Berweger, S.; Wei, J.; Cobden, D.; Raschke, M. B. *Nano Lett.* **2010**, *10*, 1574–1581.

[13] Eisele, M.; Cocker, T. L.; Huber, M. A.; Plankl, M.; Viti, L.; Ercolani, D.; Sorba, L.; Vitiello, M. S.; Huber, R. *Nat. Photon.* **2014**, *8*, 841–845.